



Numerically exact path-integral simulation of nonequilibrium quantum transport and dissipation

Dvira Segal

Chemical Physics Theory Group, Department of Chemistry, University of Toronto, Toronto, Ontario, Canada M5S 3H6

Andrew J. Millis

Department of Physics, Columbia University, 538 W 120th Street, New York, New York 10027, USA

David R. Reichman

Department of Chemistry, Columbia University, 3000 Broadway, New York, New York 10027, USA

(Received 30 August 2010; published 18 November 2010)

We develop an iterative, numerically exact approach for the treatment of nonequilibrium quantum transport and dissipation problems that avoids the real-time sign problem associated with standard Monte Carlo techniques. The method requires a well-defined decorrelation time of the nonlocal influence functional for proper convergence to the exact limit. Since finite decorrelation times may arise either from temperature *or from a voltage drop* at zero temperature, the approach is well suited for the description of the real-time dynamics of single-molecule devices and quantum dots driven to a steady state via interaction with two or more electron leads. We numerically investigate two nontrivial models: the evolution of the nonequilibrium population of a two-level system coupled to two electronic reservoirs, and quantum transport in the nonequilibrium Anderson model. For the latter case, two distinct formulations are described. Results are compared to those obtained by other techniques.

DOI: [10.1103/PhysRevB.82.205323](https://doi.org/10.1103/PhysRevB.82.205323)

PACS number(s): 05.60.Gg, 03.65.Yz, 72.10.Fk, 73.63.-b

I. INTRODUCTION

There are several ways in which a quantal entity may exhibit nontrivial departures from equilibrium. First, a system may evolve toward equilibrium after application of a transient external pulse or from a nonequilibrium initial condition. Simple examples of such situations are now relatively well understood.^{1,2} Related to these types of departures from equilibrium, but less well understood, are more challenging cases of “quantum quenches,” whereby the sudden change in a control parameter induces dynamics that probe nontrivial aspects of strong correlation or quantum criticality.³ Also underdeveloped is our understanding of quantum mechanical systems driven to nonequilibrium steady states via coupling to two or more electronic reservoirs. Since this is the case of direct relevance for the study of transport through quantum dots and molecular electronic devices,^{4,5} the complete description of this type of nonequilibrium behavior is of practical as well as fundamental interest.

There are essentially two main theoretical frameworks for the calculation of properties related to the approach to, and attainment of, nonequilibrium steady states of the types mentioned above. The first is the standard real-time Schwinger-Keldysh technique.⁶ This approach has led to the exact formulation of steady-state properties (e.g., the current) in terms of Keldysh Green’s functions.⁷ A variety of direct perturbative and renormalization-group calculations have naturally emerged from this starting point.^{8–10} In addition, real-time Monte Carlo (MC) methods have been formulated on the basis of the Schwinger-Keldysh approach.^{11–13} The Monte Carlo methods are exact in principle but may be severely limited by numerical sign problems, depending on the formulation, system, and regime under investigation.

The second framework involves the use of Lippmann-Schwinger scattering states¹⁴ to construct the properties of

nonequilibrium quantum steady state. This approach has led to several rigorous results for integrable models.¹⁵ In the last few years this viewpoint, combined with the notion of Hershfield’s steady-state density operator,¹⁶ has inspired the formulation of new nonperturbative approaches as well as numerical methods.^{17–20} Most recently, promising numerical renormalization-group approaches have been put forward based directly on the construction of scattering states,²¹ and an extension to the density-matrix renormalization-group method, incorporating real-time evolution, has been presented.^{22,23}

Consideration of more standard classes of nonequilibrium relaxation in dissipative systems such as the spin-boson model has led to a variety of path-integral techniques for the numerically exact propagation of the reduced density matrix of a small system coupled to its environment.¹ These methods, which include real-time Monte Carlo techniques¹¹ as well as deterministic iterative approaches,^{24–26} are connected to the Schwinger-Keldysh-type framework discussed above. Here, as in the Schwinger-Keldysh technique, the approach to equilibrium along a particular time contour from a prescribed nonequilibrium initial condition is described. Of these approaches, iterative path-integral methods have had particular success.²⁴ Such methods are based on the notion that a well-defined bath correlation time (if one exists) renders the range of the influence functional (IF) finite, allowing for a controlled truncation of memory effects and thus a deterministic propagation of observables that is free of the real-time sign problem.

While iterative path-integral approaches have been proven successful in describing nonequilibrium dynamics in simple spin-boson type models in the last 15 years, only recently they have been formulated and used in cases of relevance to transport through quantum dots and molecular electronic

devices.²⁷ In such systems, given that a chemical potential difference between electronic reservoirs leads to a well defined decorrelation time for dynamics *even at zero temperature*, a memory time, beyond which correlations can be dropped, exists. This finite-memory characteristic allows the development of iterative techniques, capable of describing relaxation in a wide and nontrivial region of parameter space.

In this work we develop and apply a new iterative path-integral technique to two models of nonequilibrium transport and dissipation: the spin-fermion (SF) model and the single-impurity Anderson model (SIAM). The techniques developed here hold the potential for the exact description of long-time dynamics in systems driven to a nonequilibrium steady state via coupling to two or more electronic reservoirs. The method we describe in this work is conceptually similar to the iterative summation of real-time path integrals (ISPI) approach of Thorwart and co-workers.²⁷ The distinction between these two approaches lies mainly in the propagation scheme and the manner in which the leads are traced out of the problem. In the iterative approach developed here, the reservoirs are represented as discrete levels and are eliminated numerically via the Blankenbecler-Scalapino-Sugar (BSS) identity.²⁸ While this approach has the disadvantage that an additional source of systematic error is introduced due to the discretization of the lead degrees of freedom, we find empirically that the error is easily controlled without undue computational expense. The advantage of this approach is that the study of general models (for example, multisite Hubbard “dots”) may be performed with essentially no reformulation of methodology. Taking advantage of this fact, we present a first set of exact results for the out-of-equilibrium two-lead spin-fermion model. A second difference between the ISPI approach and the approach outlined in this work is related to the propagation scheme. Here we combine our matrix formulation with a propagation scheme similar to that described in Ref. 26. This allows for very efficient propagation that may be trivially parallelized with commercially available software.²⁹ These distinctions in scaling and flexibility of approach render our formulation as a useful complement to the previously developed ISPI method.

This paper is organized as follows. Section II and Appendix A present some general aspects of the iterative propagation technique. Section III contains a case study of the relaxation of a tunneling system coupled to two electronic reservoirs. In Sec. IV we investigate nonequilibrium transport through an Anderson dot. In Sec. V we conclude. Appendix B describes extensions to nonzero temperatures. We include an alternative formulation of our approach for the nonequilibrium Anderson dot in Appendix C. This formulation may also hold promise in related path-integral approaches such as the ISPI approach. Finally, Appendix D discusses some aspects of the convergence analysis which is necessary for elimination of the systematic errors in the method.

II. GENERAL FORMULATION OF THE ITERATIVE APPROACH

We consider a generic many-body system, consisting of a finite interacting region coupled to two infinite noninteract-

ing reservoirs. The Hamiltonian H can be partitioned into a zeroth-order term H_0 whose solution can be exactly obtained, typically containing few-body interactions, and a higher order interaction term H_1 . We introduce our iterative approach using the reduced density matrix, $\rho_S = \text{Tr}_B\{\rho\}$, obtained by tracing the total density matrix ρ over the reservoir degrees of freedom. The time evolution of $\rho_S(t)$ is exactly given by

$$\rho_S(s'', s'; t) = \text{Tr}_B \langle s'' | e^{-iHt} \rho(0) e^{iHt} | s' \rangle. \quad (1)$$

We decompose the evolution operator into a product of N exponentials, $e^{iHt} = (e^{iH\delta t})^N$; $\delta t = t/N$, and define the discrete time evolution operator $\mathcal{G} \equiv e^{iH\delta t}$. Different Trotter decompositions can be employed for splitting this operator. For example, we find it convenient to approximate $\mathcal{G} \sim e^{iH_1\delta t/2} e^{iH_0\delta t} e^{iH_1\delta t/2}$ when studying the spin-fermion model (Sec. III) while for the Anderson model (Sec. IV) we find that it is useful to employ a decomposition of the form $\mathcal{G} \sim e^{iH_0\delta t/2} e^{iH_1\delta t} e^{iH_0\delta t/2}$. The overall time evolution can be represented in a path-integral formulation,

$$\begin{aligned} \rho_S(s'', s', t) = & \int ds_0^+ \int ds_1^+ \cdots \int ds_{N-1}^+ \\ & \times \int ds_0^- \int ds_1^- \cdots \int ds_{N-1}^- \text{Tr}_B \{ \langle s'' | \mathcal{G}^\dagger | s_{N-1}^+ \rangle \\ & \times \langle s_{N-1}^+ | \mathcal{G}^\dagger | s_{N-2}^+ \rangle \cdots \langle s_0^+ | \rho(0) | s_0^- \rangle \cdots \langle s_{N-2}^- | \mathcal{G} | s_{N-1}^- \rangle \\ & \times \langle s_{N-1}^- | \mathcal{G} | s' \rangle \}, \end{aligned} \quad (2)$$

where s_k^\pm are subsystem (or fictitious) degrees of freedom, representing the discrete path on the forward (+) and backward (−) contours. As an initial condition we may assume that $\rho(0) = \rho_B \rho_S(0)$ with the bath (B) uncoupled to the subsystem. In what follows we refer to the integrand in Eq. (2) as an “Influence Functional,”³⁰ and denote it by $I(s_0^+, s_1^+, \dots, s_N^+; s_0^-, s_1^-, \dots, s_N^-)$, assigning $s_N^+ = s''$, $s_N^- = s'$. Note that our definition of the IF is more general than that contained in the original work of Feynman and Vernon.³⁰ We chose this loose definition to make connection with the iterative schemes developed in the previous path-integral-based numerical work.²⁴

The IF combines the information of subsystem and bath degrees of freedom with system-bath interactions, and its form is analytically known only in special cases. For example, for a harmonic bath bilinearly coupled to a subsystem the IF is an exponential of a quadratic form, multiplied by free-subsystem propagation terms³⁰

$$\begin{aligned} I^{har}(s_0^+ \cdots s_N^+; s_0^- \cdots s_N^-) \\ = \exp \left[- \sum_{k=0}^N \sum_{k'=0}^k (s_k^+ - s_k^-) (\eta_{k,k'} s_{k'}^+ - \eta_{k,k'}^* s_{k'}^-) \right] \\ \times \langle s_N^+ | e^{-iH_0\delta t} | s_{N-1}^+ \rangle \cdots \langle s_0^+ | \rho_S(0) | s_0^- \rangle \cdots \langle s_{N-1}^- | e^{iH_0\delta t} | s_N^- \rangle. \end{aligned} \quad (3)$$

The coefficients $\eta_{k,k'}$ depend on the bath spectral function and the temperature.²⁴ For a general anharmonic environment the IF may contain multiple-site interactions, where the coefficients are not known in general.²⁵ However, even when

the form of the IF is analytically known as in Eq. (3), it still combines long-range interactions limiting brute force direct numerical simulations to very short times.

For a system coupled to a *single* thermal reservoir this challenge has been tackled at finite temperatures where a natural bath decoherence time exists. As noted by Makri and Makarov,²⁴ such cases are characterized by the useful feature that nonlocal correlations contained in the IF decay exponentially, enabling a (controlled) truncation of the IF that includes only a finite memory length. Based on this feature, an iterative scheme for evaluating the (finite-dimensional) path integral has been developed.²⁴ While the original quasiadiabatic path-integral (QUAPI) algorithm was developed based on the analytical pairwise form of the IF specific to harmonic reservoirs [Eq. (3)], a subsequent more general approach proposed in Ref. 26 is based only on the fact that memory effects at finite temperatures generically vanish exponentially in the long-time limit.

This idea can be further employed to simulate the dynamics of a generic *nonequilibrium* bias-driven system.²⁷ Since in standard nonequilibrium situations bath correlations die exponentially, the IF can be truncated beyond a memory time $\tau_c = N_s \delta t$, corresponding to the time where beyond which bath correlations may be controllably ignored. Here, N_s is an integer, δt is the discretized time step, and τ_c is a correlation time dictated by the nonequilibrium situation. For a system under a dc potential bias $\Delta\mu$ at zero temperature, $\tau_c \sim 1/\Delta\mu$, while at temperatures for which $T > \Delta\mu$ temperature sets the scale of the memory range. We therefore write the total influence functional approximately as

$$\begin{aligned} I(s_0^\pm, s_1^\pm, s_2^\pm, \dots, s_N^\pm) \\ \approx I(s_0^\pm, s_1^\pm, \dots, s_{N_s}^\pm) I(s_1^\pm, s_2^\pm, \dots, s_{N_s+1}^\pm) \cdots \\ \times I(s_{N-N_s}^\pm, s_{N-N_s+1}^\pm, \dots, s_N^\pm) \end{aligned} \quad (4)$$

with

$$I_s(s_k^\pm, s_{k+1}^\pm, \dots, s_{k+N_s}^\pm) = \frac{I(s_k^\pm, s_{k+1}^\pm, \dots, s_{k+N_s}^\pm)}{I(s_k^\pm, s_{k+1}^\pm, \dots, s_{k+N_s-1}^\pm)}. \quad (5)$$

The errors in Eq. (4) are the usual Trotter error arising from the time discretization and the truncation to a finite memory time $\tau_c = N_s \delta t$. Both of these errors can be controlled. Equation (4) can be understood as a simple generalization of the pairwise expression (3) for which

$$I_s^{har}(s_k^\pm, s_{k+1}^\pm, \dots, s_{k+N_s}^\pm) = f_0(s_k^\pm) f_1(s_k^\pm, s_{k+1}^\pm) \cdots f_{N_s}(s_k^\pm, s_{k+N_s}^\pm). \quad (6)$$

The one-body and two-body functions f can be obtained by rearranging Eq. (3). From these expressions we recursively build the finite-range IF for a general model. We assume that the complete functional decays to zero with time constant $\tau_c = N_s \delta t$, ($N_s < N$), thus it can be approximated by the product

$$\begin{aligned} I(s_0^\pm, s_1^\pm, s_2^\pm, \dots, s_N^\pm) \\ \approx I(s_0^\pm, s_1^\pm, s_2^\pm, \dots, s_{N-1}^\pm) \frac{I(s_1^\pm, s_2^\pm, s_3^\pm, \dots, s_N^\pm)}{I(s_1^\pm, s_2^\pm, s_3^\pm, \dots, s_{N-1}^\pm)}. \end{aligned} \quad (7)$$

By recursively applying this rule, the truncated IF is further decomposed until it correlates interactions within τ_c only,

$$\begin{aligned} I(s_0^\pm, s_1^\pm, s_2^\pm, \dots, s_N^\pm) \approx I(s_0^\pm, s_1^\pm, \dots, s_{N_s}^\pm) \\ \times \frac{I(s_1^\pm, s_2^\pm, \dots, s_{N_s+1}^\pm) I(s_2^\pm, s_3^\pm, \dots, s_{N_s+2}^\pm)}{I(s_1^\pm, s_2^\pm, \dots, s_{N_s}^\pm) I(s_2^\pm, s_3^\pm, \dots, s_{N_s+1}^\pm)} \cdots \\ \times \frac{I(s_{N-N_s}^\pm, s_{N-N_s+1}^\pm, \dots, s_N^\pm)}{I(s_{N-N_s}^\pm, s_{N-N_s+1}^\pm, \dots, s_{N-1}^\pm)}, \end{aligned} \quad (8)$$

resulting in Eqs. (4) and (5). The physical content of this approach, which is similar to that described in Ref. 26, is outlined in Appendix A. The approach becomes exact as $\tau_c \rightarrow \infty$. Outside of the initial propagation step, $I_s(s_0^\pm, s_1^\pm, \dots, s_{N_s}^\pm) \equiv I(s_0^\pm, s_1^\pm, \dots, s_{N_s}^\pm)$, we can identify the functions I_s [Eq. (4)] as the ratio between two IFs where the numerator is calculated with an additional time step, Eq. (5). Next, based on the decomposition [Eq. (4)] we can iteratively integrate Eq. (2) by defining a multiple-time reduced density matrix $\tilde{\rho}_S(s_k, s_{k+1}, \dots, s_{k+N_s-1})$. Its initial value is given by $\tilde{\rho}_S(s_0^\pm, \dots, s_{N_s-1}^\pm) = I$, and its evolution is dictated by

$$\tilde{\rho}_S(s_1^\pm, \dots, s_{N_s}^\pm) = \int ds_0^\pm \tilde{\rho}_S(s_0^\pm, \dots, s_{N_s-1}^\pm) I_s(s_0^\pm, \dots, s_{N_s}^\pm) \quad (9)$$

with

$$\begin{aligned} I_s(s_0^\pm, \dots, s_{N_s}^\pm) = \text{Tr}_B \{ \langle s_{N_s}^\pm | \mathcal{G}^\dagger | s_{N_s-1}^\pm \rangle \cdots \langle s_1^\pm | \mathcal{G}^\dagger | s_0^\pm \rangle \langle s_0^\pm | \rho(0) | s_0^\pm \rangle \\ \times \langle s_0^- | \mathcal{G} | s_1^- \rangle \cdots \langle s_{N_s-1}^- | \mathcal{G} | s_N^- \rangle \}. \end{aligned} \quad (10)$$

A general propagation step involves integration over two (\pm) coordinates,

$$\tilde{\rho}_S(s_{k+1}^\pm, \dots, s_{k+N_s}^\pm) = \int ds_k^\pm \tilde{\rho}_S(s_k^\pm, \dots, s_{k+N_s-1}^\pm) I_s(s_k^\pm, \dots, s_{k+N_s}^\pm), \quad (11)$$

where the time-local ($t_k = k \delta t$) reduced density matrix is obtained by summing over all intermediate states,

$$\rho_S(t_k) = \int ds_{k-1}^\pm \cdots ds_{k-N_s+1}^\pm \tilde{\rho}_S(s_{k-N_s+1}^\pm, \dots, s_k^\pm). \quad (12)$$

The evolution at shorter times $k < N_s$ can be calculated in a numerically exact way. Before turning to specific models we would like to make the following comments regarding the above derivation. (i) The specific partitioning of the Hamiltonian into H_0 and H_1 depends on the model investigated. As we show below, H_0 may include only the subsystem degrees of freedom (spin-fermion model) or it may be constructed involving all two-body terms (Anderson model). (ii) Obviously, the decomposition [Eq. (7)] is not unique, however,

different schemes should lead to equivalent time evolution, and thus the partitioning is a matter of numerical convenience. (iii) The truncated IF (I_S) is not necessarily a time invariant. As we show below, in the spin-fermion model I_S does not depend on time, thus in this case it needs to be evaluated only once during the propagation scheme. In contrast for the Anderson model standard use of the Hubbard-Stratonovich (HS) transformation leads to an IF expression that has to be updated at each time step. In Appendix C we outline an approach that does not make use of the Hubbard-Stratonovich transformation and thus produces a form on the IF of the Anderson model that is time independent. (iv) The short-range function I_S can be analytically evaluated in some special cases.^{24,25} For general reservoirs it may be evaluated numerically, by using finite-size reservoirs as described in the next section. (v) The approach outlined here is not restricted to specific statistics of the leads (boson or fermion) and is solely based on the fact that at finite temperature and/or finite bias bath correlations exponentially decay at long time. Therefore, it can be used to treat finite temperature anharmonic bosonic environments²⁶ as well as nonequilibrium Fermi systems.

III. DISSIPATION IN THE NONEQUILIBRIUM SPIN-FERMION MODEL

A. Model

As a first example, we consider the dynamics of a two-state system coupled to two fermionic leads maintained at different chemical potential values, the ‘‘Spin Fermion model.’’ This model has been considered in a series of recent papers,^{31–34} and serves as a simple, albeit nontrivial, example exhibiting the generic behavior associated with the approach to a nonequilibrium steady state. In particular, at zero temperature the chemical-potential difference $\Delta\mu$ sets the essential energy scale for dephasing as is expected generically in more complex models such as the nonequilibrium Kondo model.³⁵ It should be noted, however, the connection between the model studied here and the nonequilibrium Kondo model³⁵ is more tenuous than that between the tunneling center model in equilibrium¹ and the standard (equilibrium) Kondo model.³⁶ We take as our Hamiltonian

$$H^{\text{SF}} = H_0 + H_1,$$

$$H_0 = H_S, \quad H_1 = H_B + H_{SB}. \quad (13)$$

The bath Hamiltonian H_B is taken to be that of two independent leads ($\alpha=L,R$) characterized by (spinless) free-fermion statistics with different chemical potentials, namely,

$$H_B = \sum_{\alpha,k} \epsilon_k c_{\alpha,k}^\dagger c_{\alpha,k}. \quad (14)$$

The operator $c_{\alpha,k}^\dagger$ ($c_{\alpha,k}$) creates (annihilates) an electron with momentum k in the α th lead. The system Hamiltonian H_S consists of a two-level system with a bare tunneling amplitude Δ and a level splitting B ,

$$H_S = \frac{B}{2} \sigma_z + \frac{\Delta}{2} \sigma_x. \quad (15)$$

We take the general form for the system-bath coupling to be

$$H_{SB} = \sum_{\alpha,\alpha',k,k'} V_{\alpha,k;\alpha',k'} c_{\alpha,k}^\dagger c_{\alpha',k'} \sigma_z. \quad (16)$$

Different versions of the model may be expressed via different forms of the coupling parameters V . In this paper we focus on the model presented in Refs. 32 and 37, where the momentum dependence of the scattering potential is neglected. The system-bath scattering potentials are then given by $V_{\alpha,\alpha'}$, where $\alpha, \alpha' = L, R$ are the Fermi sea indices.

In the standard application of iterative path-integral approaches, two features greatly simplify the propagation algorithm. First, the form of the Feynman-Vernon influence functional is known analytically. Second, the influence functional is pairwise decomposable.²⁴ As discussed in the previous section, neither of these features is necessary for the numerical implementation of an efficient iterative routine.

Recently, the analytical structure of the influence functional in the spin-fermion model considered here has been elucidated, with a modified pairwise Coulomb gas behavior emerging at long times.³³ However, our recent numerical results have illustrated that in some cases for strong coupling of the system to the leads, most of the relevant dynamical evolution occurs in time intervals *before* strict Coulomb gas behavior holds.³²

The exact dynamics follows Eq. (2). Assuming separable initial conditions $\rho(t=0) = \rho_S(t=0)\rho_B(t=0)$, we can identify the IF in the present model as

$$\begin{aligned} I(s_0^\pm, s_1^\pm, \dots, s_N^\pm) &= \langle s_0^\pm | \rho_S(0) | s_0^\mp \rangle \\ &\times K(s_N^\pm, s_{N-1}^\pm) \cdots K(s_2^\pm, s_1^\pm) K(s_1^\pm, s_0^\pm) \\ &\times \text{Tr}_B \{ e^{-iH_1(s_N^\pm)\delta t/2} e^{-iH_1(s_{N-1}^\pm)\delta t} \dots \\ &\times e^{-iH_1(s_0^\pm)\delta t/2} \rho_B(0) e^{iH_1(s_0^\mp)\delta t/2} \dots \\ &\times e^{iH_1(s_{N-1}^\mp)\delta t} e^{iH_1(s_N^\mp)\delta t/2} \}. \end{aligned} \quad (17)$$

where $H_1 = H_B + H_{SB}$ provides an adiabatic partitioning of the Hamiltonian, s_k^\pm are forward (+) and backward (−) spin states along the paths, and $K(s_{k+1}^\pm, s_k^\pm) = \langle s_{k+1}^\pm | e^{-iH_S \delta t} | s_k^\pm \rangle \langle s_k^\mp | e^{iH_S \delta t} | s_{k+1}^\mp \rangle$ is the propagator matrix for the isolated subsystem.

The reduced density matrix is time propagated by employing the iterative scheme [Eqs. (9)–(12)], where the function I_S [Eq. (5)] is calculated by taking ratios of the corresponding truncated IF [Eq. (17)]. Note that this function is time-translationally invariant, thus we need to calculate it only once.

B. Results

To numerically calculate the influence functional, we express the lead Hamiltonians in terms of a finite number of fermions. Then, as in the standard BSS Monte Carlo approach to lattice fermions,²⁸ the resulting trace may be expressed as a simple determinant containing the one-body ma-

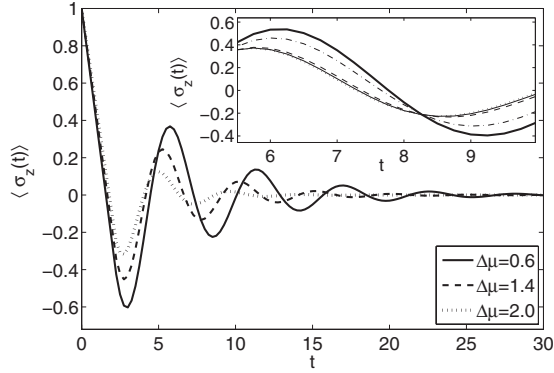


FIG. 1. Polarization in the nonequilibrium spin-fermion model at different values of the bias voltage $\Delta\mu=0.6$ (full); $\Delta\mu=1.4$ (dashed); and $\Delta\mu=2$ (dotted), $B=0$, $\Delta=1$, $\lambda=0.2$, $\delta t=0.25$, and $N_s=8$. Inset: convergence with increasing correlation time at $\Delta\mu=0.6$, $N_s=3$ (dark full); $N_s=4$ (dashed-dotted); $N_s=7$ (dashed); $N_s=8$ (dotted); and $N_s=9$ (light full). Data were generated using 80 states per bath, which is sufficient to ensure convergence in the regime of parameters presented here.

trices that represent exponentials of operators that are quadratic in fermionic creation and annihilation operators. It should be noted that this discretization of the bath leads to systematic error in the results, unlike the case for the related ISPI approach of Thorwart and co-workers.²⁷ However, the discretized approach for tracing out the bath is more flexible in that cases where the analytic structure of the self-energy terms, such as structured “dot” with several correlated sites, may be easily treated. Furthermore, bosonic analogs of generalized Anderson models may be treated easily as well,³⁸ using the boson version of the BSS formalism.³⁹ This fact may be of importance for the recently developed bosonic versions of dynamical mean field theory (DMFT),^{40,41} where for out-of-equilibrium situations or at finite temperatures the approach outlined here may potentially serve as a real-time impurity solver. Fortunately, since the time intervals over which the bath is “measured” are short, we have found that the infinite bath result is easily reached even with a relatively small number of effective bath fermions ~ 40 .

We use the following parameters: $\Delta=1$, $B=0$, $\Delta\mu \sim 0.5-2$, and $\rho V_{\alpha,\alpha'} = \lambda(1 - \delta_{\alpha,\alpha'})$, considering only interbath system-bath couplings, where spin polarization is coupled to scattering events between the nonequilibrium reservoirs. Here ρ denotes the density of states of each Fermi sea. For simplicity we assume zero temperature. The generalization to finite temperature is straightforward as outlined in Appendix B. Since the iterative approach outlined above requires a finite range of memory for the influence functional, we work with a bias large enough to ensure facile convergence in the numerical examples outlined below.

In Fig. 1 we show the dynamics of the spin polarization $\langle \sigma_z(t) \rangle$ for several different values of the bias $\Delta\mu$, distributed symmetrically between the L and R leads. The role of the chemical-potential difference as a temperature like contributor to dephasing is clear.³² We analyze (inset) the memory error in our algorithm by increasing τ_c , keeping δt fixed. As expected, we find that τ_c roughly corresponds to $1/\Delta\mu$. Thus, for $\Delta\mu \sim 1$, taking $\delta t=0.25$, the dynamics is converg-

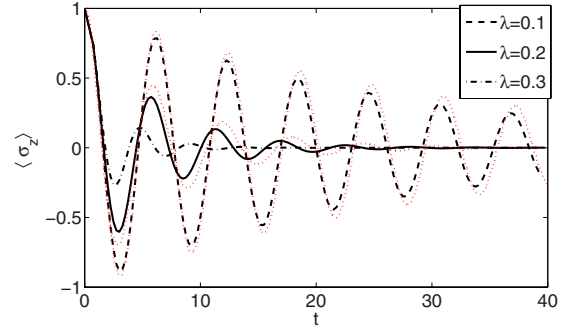


FIG. 2. (Color online) Polarization in the nonequilibrium spin-fermion model at different spin-bath couplings, $\lambda=0.1$ (dashed); $\lambda=0.2$ (full); and $\lambda=0.3$ (dashed-dotted). Here $\Delta\mu=0.6$ and $\delta t=0.25$, $N_s=10$. The dotted line was generated using a nonequilibrium version of the “noninteracting spin-blip approximation” (Refs. 31 and 32).

ing for $N_s \geq 5$. A complete discussion of the appropriate convergence analysis is presented in Appendix D for the Anderson model.

In Fig. 2 we compare our numerically exact results, with the results of a generalized “noninteracting blip” approximation as formulated by Mitra and Millis.^{31,32} While at weak coupling the dynamics reasonably agree, for strong interactions $\lambda=0.3$ ($\pi\rho V_{\alpha,\alpha'} \sim 1$) the perturbative method diverges.³² We found that at weak to intermediate interaction strengths our results systematically converge with increasing memory time τ_c . For strong interactions $\pi\delta \sim 1$ the time step in our simulations should be made further smaller $\delta t \sim 0.1$ in order to achieve convergence, demanding extensive computation effort as $N_s > 16$ for $\Delta\mu \sim 0.6$.

It would be most useful to undertake a systematic study of the dynamical phase diagram in $(T, \Delta\mu, \rho V_{\alpha,\alpha'})$ space in the regions where our iterative technique is convergent. Such a study would be quite useful for the understanding of the approach to nonequilibrium steady state and will be the subject of a future investigation.

IV. NONEQUILIBRIUM TRANSPORT THROUGH AN ANDERSON DOT

A. Method

The single impurity Anderson model (SIAM) (Ref. 42) is one of the most important and well-studied models in condensed matter physics. While it was originally introduced to describe the behavior of magnetic impurities in nonmagnetic hosts,³⁶ it has more recently served as a general model for understanding transport in correlated nanoscale systems.^{4,5} In such cases, the impurity is hybridized with more than one reservoir, and if the chemical potentials of the reservoirs are not identical, nonequilibrium transport will occur. Here, we present a numerically exact scheme for calculating dynamical quantities such as the time-dependent occupation and current in such systems. The approach outlined in this section relies on the discrete HS transformation. An alternative and more general approach is outlined in Appendix C that does not employ this transformation. While the approach of Ap-

pendix C offers several advantages, it is somewhat simpler to implement the scheme described here, and for that reason we follow it for the sake of illustrative calculation.

The SIAM model includes a resonant level of energy ϵ_d , described by the creation operator d_σ^\dagger ($\sigma = \uparrow, \downarrow$ denotes the spin orientation) coupled to two fermionic leads ($\alpha = L, R$) of different chemical potentials μ_α ,

$$H^{AM} = \sum_{\sigma} \epsilon_d d_\sigma^\dagger d_\sigma + U d_\uparrow^\dagger d_\downarrow^\dagger d_\uparrow d_\downarrow + \sum_{\alpha, k, \sigma} \epsilon_k c_{\alpha, k, \sigma}^\dagger c_{\alpha, k, \sigma} + \sum_{\alpha, k, \sigma} V_{\alpha, k} c_{\alpha, k, \sigma}^\dagger d_\sigma + \text{H.c.} \quad (18)$$

Here $c_{\alpha, k, \sigma}^\dagger$ ($c_{\alpha, k, \sigma}$) denotes the creation (annihilation) of an electron with momentum k and spin σ in the α lead, U stands for the onsite repulsion energy, and $V_{\alpha, k}$ are the impurity- α lead coupling elements. Hamiltonian (18) can be also rewritten as $H^{AM} = H_0 + H_1$, where H_0 includes the exactly solvable noninteracting part, and H_1 includes the many-body term,

$$H_0 = \sum_{\sigma} (U/2 + \epsilon_d) d_\sigma^\dagger d_\sigma + \sum_{\alpha, k, \sigma} \epsilon_k c_{\alpha, k, \sigma}^\dagger c_{\alpha, k, \sigma} + \sum_{\alpha, k, \sigma} V_{\alpha, k} c_{\alpha, k, \sigma}^\dagger d_\sigma + \text{H.c.},$$

$$H_1 = U \left[n_{d, \uparrow} n_{d, \downarrow} - \frac{1}{2} (n_{d, \uparrow} + n_{d, \downarrow}) \right]. \quad (19)$$

Here $n_{d, \sigma} = d_\sigma^\dagger d_\sigma$ is the impurity occupation number operator. The shifted single-particle energies are denoted by $E_d = \epsilon_d + U/2$. We also define $\Gamma = \sum_{\alpha} \Gamma_{\alpha}$, where $\Gamma_{\alpha} = \pi \sum_k |V_{\alpha, k}|^2 \delta(\epsilon - \epsilon_k)$ is the hybridization energy of the resonant level with the α metal.

Our objective is to calculate the dynamics of a quadratic operator \hat{A} , either given by system or bath degrees of freedom. This can be generally done by studying the Heisenberg

equation of motion of the exponential operator $e^{\lambda \hat{A}}$ with λ here a variable that is taken to vanish at the end of the calculation,

$$\langle \hat{A}(t) \rangle = \text{Tr}(\rho \hat{A}) = \lim_{\lambda \rightarrow 0} \frac{\partial}{\partial \lambda} \text{Tr}[\rho(0) e^{iH^{AM}t} e^{\lambda \hat{A}} e^{-iH^{AM}t}]. \quad (20)$$

Here ρ is the total density matrix. For simplicity, we assume that at the initial time ($t=0$) the dot and the bath are decoupled, the impurity site is empty, and the bath is prepared in a nonequilibrium (biased) zero-temperature state. The time evolution of \hat{A} can be obtained following a scheme analogous to that outlined in Sec. II for the reduced density matrix. For clarity, we rederive an explicit expression for the generalized IF in the present case as well.

First we use a standard factorization of the time evolution operator $e^{iH^{AM}t} = (e^{iH^{AM}\delta t})^N$, and assume the Trotter decomposition $e^{iH^{AM}\delta t} \approx (e^{iH_0\delta t/2} e^{iH_1\delta t} e^{iH_0\delta t/2})$. The many body term H_1 is further eliminated by introducing auxiliary Ising variables $s = \pm$ via the Hubbard-Stratonovich transformation,⁴³

$$e^{iH_1\delta t} = \frac{1}{2} \sum_s e^{-s\kappa_+(n_{d, \uparrow} - n_{d, \downarrow})},$$

$$e^{-iH_1\delta t} = \frac{1}{2} \sum_s e^{-s\kappa_-(n_{d, \uparrow} - n_{d, \downarrow})}, \quad (21)$$

where $\kappa_{\pm} = \kappa' \mp i\kappa''$, $\kappa' = \sinh^{-1}[\sin(\delta t U/2)]^{1/2}$, and $\kappa'' = \sin^{-1}[\sin(\delta t U/2)]^{1/2}$. The uniqueness of this transformation requires $U\delta t < \pi$. In what follows we use the following notation:

$$e^{H_{\pm}(s)} \equiv e^{-s\kappa_{\pm}(n_{d, \uparrow} - n_{d, \downarrow})}. \quad (22)$$

Incorporating the Trotter decomposition and the HS transformation [Eq. (22)] into Eq. (20), we find that at zero temperature the time evolution of \hat{A} is given by

$$\langle \hat{A}(t) \rangle = \lim_{\lambda \rightarrow 0} \frac{\partial}{\partial \lambda} \langle 0 | (e^{iH_0\delta t/2} e^{iH_1\delta t} e^{iH_0\delta t/2})^N e^{\lambda \hat{A}} (e^{-iH_0\delta t/2} e^{-iH_1\delta t} e^{-iH_0\delta t/2})^N | 0 \rangle$$

$$= \lim_{\lambda \rightarrow 0} \frac{\partial}{\partial \lambda} \left\{ \frac{1}{2^{2N}} \int ds_1^{\pm} ds_2^{\pm} \cdots ds_N^{\pm} \langle 0 | (e^{iH_0\delta t/2} e^{H_+(s_N^{\pm})} e^{iH_0\delta t/2}) \cdots (e^{iH_0\delta t/2} e^{H_+(s_1^{\pm})} e^{iH_0\delta t/2}) e^{\lambda \hat{A}} \right.$$

$$\left. \times (e^{-iH_0\delta t/2} e^{H_-(s_1^{\mp})} e^{-iH_0\delta t/2}) \cdots (e^{-iH_0\delta t/2} e^{H_-(s_N^{\mp})} e^{-iH_0\delta t/2}) | 0 \rangle \right\}, \quad (23)$$

where $|0\rangle$ is the initial (zero-temperature) state of the total system. For convenience, we evaluate Eq. (23) by diagonalizing the Hamiltonian H_0 [see Eq. (19)], and rewriting H_{\pm} in terms of the new basis

$$\begin{aligned}\bar{H}_0 &= \sum_{\nu} \epsilon_{\nu} b_{\nu}^{\dagger} b_{\nu}, & H_0 &= V \bar{H}_0 V^{-1}, \\ \bar{H}_{\pm} &= \sum_{\nu, \nu'} \beta_{\nu}^* \beta_{\nu'} b_{\nu}^{\dagger} b_{\nu'}\end{aligned}\quad (24)$$

with β_{ν} as the transformation matrix elements. We further transform both the operator of interest and the ground state into the new representation $\hat{A} = V \bar{A} V^{-1}$, $|\bar{0}\rangle = V^{-1}|0\rangle$. The IF is identified as the integrand in Eq. (23), where we truncate interactions beyond the memory time $\tau_c = N_s \delta t$,

$$\begin{aligned}I(s_k^{\pm}, \dots, s_{k+N_s}^{\pm}) &= \frac{1}{2^{2N_s+2}} \langle \bar{0} | \mathcal{G}_+(s_{k+N_s}^+) \cdots \mathcal{G}_+(s_k^+) \\ &\quad \times e^{i\bar{H}_0(k-1)\delta t} e^{\lambda \bar{A}} e^{-i\bar{H}_0(k-1)\delta t} \\ &\quad \times \mathcal{G}_-(s_k^-) \cdots \mathcal{G}_-(s_{k+N_s}^-) | \bar{0} \rangle\end{aligned}\quad (25)$$

with $\mathcal{G}_+(s_k^{\pm}) = (e^{i\bar{H}_0 \delta t/2} e^{\bar{H}_{\pm}(s_k^{\pm})} e^{i\bar{H}_0 \delta t/2})$ and $\mathcal{G}_- = \mathcal{G}_+^{\dagger}$. Finally, we can build the function I_s [Eq. (4)] using Eq. (5), and the operator of interest \hat{A} may be propagated using a scheme analogous to that developed for the reduced density matrix, Eqs. (9)–(12).

Before presenting numerical results we make the following comments. First, in the present scheme the IF needs to be updated at each time step since the truncated IF [Eq. (25)] explicitly depends on the present time $t_k = k \delta t$. Second, the operator \hat{A} can represent various quadratic operators. Thus quantities such as the impurity population or the current through the junction¹² may be investigated on the same footing.

B. Results

The IF [Eq. (25)] is the core of our calculation. It is evaluated numerically using the zero-temperature relationship $\langle 0 | e^B | 0 \rangle = \det[e^B]_{occ.}$, where b is a single-particle operator, $B = \sum b$, and the determinant is carried over occupied states only. Extensions to finite temperature are standard, see Appendix B. Similarly to the spin-fermion model we represent the reservoirs by a finite set of fermions, with energies determined by the metals' dispersion relation. Calculations must be converged with respect to the number of discrete lead states. The λ derivative in Eq. (23) is handled numerically, by calculating the IF for several (small) values of λ .

In the following we typically use the following conventions and parameters: a symmetrically distributed voltage bias between two leads with $\Delta\mu = 0.4$ – 0.6 , a reservoir bandwidth of $D = 1$, a resonant level energy $E_d = 0.3$, and hybridization strength $\Gamma_{\alpha} = 0.025$ – 0.1 . Note that the actual hybridization parameter utilized in the simulations is the coupling $V_{\alpha,k} = \sqrt{\Gamma_{\alpha}/\pi\rho_{\alpha}}$, where ρ_{α} is the density of states of the α lead. For these parameters we find that convergence is

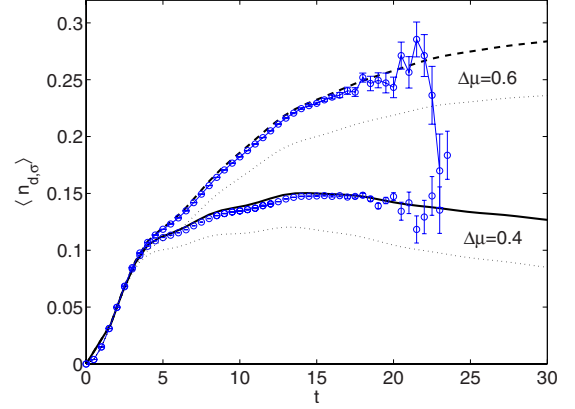


FIG. 3. (Color online) Resonant level dynamics at different values of the voltage bias, $\Delta\mu = 0.6$ (dashed) and $\Delta\mu = 0.4$ (full). $U = 0.1$, $\Gamma_{\alpha} = 0.025$, $E_d = 0.3$, and $\tau_c = 3.2$. The dotted lines show for reference the exact $U = 0$ dynamics at $\Delta\mu = 0.6$ and 0.4 (top to bottom). The circles are the respective Monte Carlo points. Calculations are performed at $T = 0$ while Monte Carlo data utilizes $T = 1/200$ which is effectively converged to the $T = 0$ limit.

achieved using $L \leq 240$ states per spin per bath. We have also verified that for $\Delta\mu = 0.4$ the memory time $\tau_c \sim 3.2$ leads to convergence with $\delta t = 0.8$ and $N_s = 4$, provided $\frac{U}{\Gamma} \leq 3$ (see Appendix D).

We begin by investigating the dynamics for a relatively small interaction $U = 0.1$ ($\Gamma \equiv \Gamma_L + \Gamma_R$ and $U/\Gamma = 2$). In this regime we are able to systematically converge the results of our procedure with respect to the three sources of systematic error, namely those associated with time step and bath discretization as well as nonlocal memory truncation. Figure 3 presents the time evolution of the dot occupation for two different bias voltages, $\Delta\mu = 0.6$ (dashed) and $\Delta\mu = 0.4$ (full), assuming the dot ($E_d = 0.3$) is initially empty. The results are compared to exact real-time MC simulations employing the hybridization expansion⁴⁴ manifesting good agreement at this relatively small U : at short times the IF data reproduce the MC features while close to steady state the MC results become increasingly unstable. The more recently developed weak-coupling expansion⁴⁵ is capable of significantly extending the time regime for which converged results may be obtained via Monte Carlo for symmetric cases, however this restriction limits the cases for which long-time results may be obtained. The MC data presented in this paper were generated at finite low temperature, $1/T = 200$. We have verified (data not included) that for this temperature range the population dynamics essentially coincide with the strictly zero-temperature case. The extremely small deviations between MC data and our approach at $U = 0.1$ in Fig. 3 are the result of small differences in temperature and the fact that a sharp, finite band is assumed in our calculations.

Figure 4 presents the time evolution of $\langle n_{d,\sigma} \rangle$ with increasing on-site interaction. While we have not been able to overcome convergence issues for all times and all values of $\frac{U}{\Gamma}$, we find that dynamics are faithfully reproduced for all $\frac{U}{\Gamma}$ at short times while accurate and converged results are correctly obtainable only for $\frac{U}{\Gamma} \leq 3$. The strict requirements for convergence are presented in Appendix D. While this regime

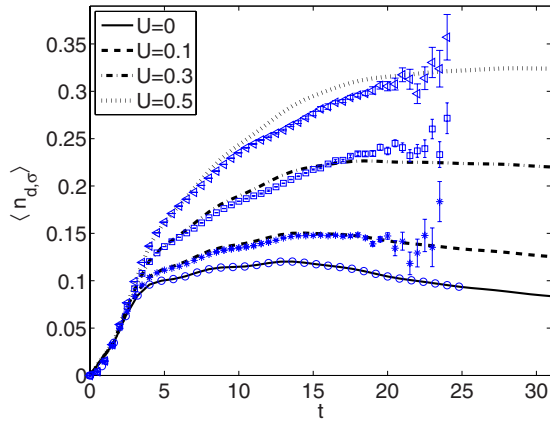


FIG. 4. (Color online) Population of the resonant level in the Anderson model. The results for $U=0$ (full), $U=0.1$ (dashed), $U=0.3$ (dashed-dotted), and $U=0.5$ (dotted) are compared with the exact dynamics at $U=0$ (\circ) and Monte Carlo data ($*$, \square , and \triangleleft). The physical parameters of the model are $D=1$, $\Delta\mu=0.4$, $E_d=0.3$, and $\Gamma_\alpha=0.025$. The numerical parameters used are $L=240$ lead states, $\tau_c=3.2$ with $N_s=4$ and $\delta t=0.8$. Note that convergence and thus agreement with Monte Carlo cannot be achieved for $t \geq 10$ if $\frac{U}{\Gamma} \geq 3$.

is one where perturbation theory in U is accurate,^{45,46} we believe that convergence restrictions are surmountable within the methodology presented in this work. Future study will be devoted to this issue. Figure 5 compares the early propagation obtained within the IF approach (\square) to the MC data (\circ). Interestingly, while our approach does not capture the t^2 characteristic at $0 < t < 3$ due to the rough time discretization, the intermediate time dynamics is still correct. It should be possible to devise an adaptive time propagation scheme where the time step is increasing with time, keeping τ_c fixed. Future work will be devoted to improving convergence for large U and t . It is interesting to note that even though the results at large time and on-site energy ($U/\Gamma \geq 3$) are not converged and thus do not controllably represent a reliable estimate of population dynamics, the results are still reasonably close to the MC data even for $\frac{U}{\Gamma}=6$.

The effect of the impurity-bath hybridization strength has been also analyzed. For $\Gamma_\alpha=0.025-0.1$ and $U=0.1-0.3$ we

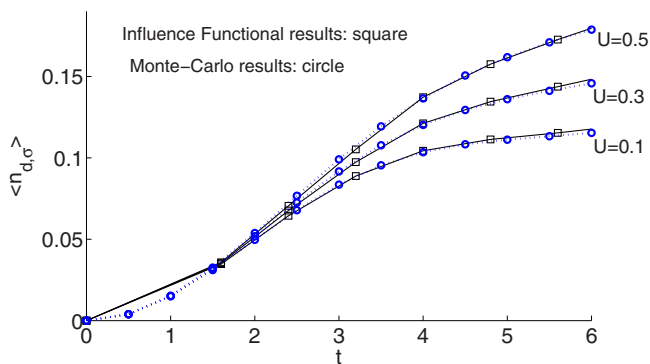


FIG. 5. (Color online) Short time dynamics in the Anderson model (\square) compared with Monte Carlo data (\circ) for $U=0.5$, 0.3 , and 0.1 (top to bottom). $D=1$, $\Delta\mu=0.4$, $E_d=0.3$, $\Gamma_\alpha=0.025$, $L=240$, and $\tau_c=3.2$ with $N_s=4$ and $\delta t=0.8$.

have obtained results in reasonable agreement with MC data, alike the behavior observed in Fig. 4. Furthermore, since our method is nonperturbative in the hybridization strength, we expect it to be useful for exploring the *nonequilibrium* Kondo effect. However, the *equilibrium* Kondo physics cannot be probed within our treatment since at low temperatures the decorrelation time required for convergence becomes too long for practical simulations.

Future work will be devoted for studying the time dependent and stationary current in the Anderson model. This can be trivially implemented using Eq. (23) with the number operator of the α lead, $\hat{A} = \sum_{k,\sigma} c_{\alpha,k,\sigma}^\dagger c_{\alpha,k,\sigma}$. The current at the α contact is then given by the time derivative $I_\alpha = \frac{d}{dt} \langle \hat{A} \rangle$. Extending the formalism to include nonzero-temperature effects is a trivial task (Appendix B). One could thus use our method for studying the thermoelectric properties of (correlated) molecular systems, a topic of recent experimental interest.⁴⁷ Note that contrary to wave function methods,⁴⁸ convergence in our scheme is facilitated by going beyond the strictly zero-temperature limit.

V. CONCLUSIONS

We have presented here a general path-integral-based iterative scheme for studying the dissipative dynamics of bias-driven nonequilibrium systems. Our method relies on the finite range of bath correlations in out-of-equilibrium cases, thus interactions within the influence functional may be truncated beyond a memory time dictated by the nonequilibrium conditions, and an iterative and deterministic scheme may be developed. This scheme is in principle exact for cases where convergence with respect to truncation of memory effects is achieved.

The philosophy of our approach is similar to the previously developed ISPI approach of Thorwart and co-workers.²⁷ The distinction between the method presented here and ISPI is confined to the propagation scheme and the technique via which the leads are eliminated. The discretized BSS-type approach²⁸ to tracing out the reservoirs used here may be employed in situations where the structure of the memory term is difficult to obtain analytically. Furthermore, the matrices involved in the iterative scheme are fixed in size, and this fact may present numerical advantages at very long times. While our approach introduces an additional source of systematic error related to discretizing the leads, we have found that this error is easily controlled with limited numerical cost. Thus, our approach presents a related but complimentary methodology to the ISPI technique. It should be noted that currently the approach presented here and the ISPI technique appear to have difficulty converging in similar regions of parameter space that are accessible in some cases by, for example, the weak-coupling Monte Carlo approach.⁴⁵ However approaches such as ISPI and the methodology presented allow for an accurate description of long-time dynamical features when they do converge, something that is generically difficult with Monte Carlo schemes. In this regard our approach is also complimentary to, and not competitive with, expansion based Monte Carlo schemes.^{44,45}

We have applied our technique to two prototype models: (i) the spin-fermion model of a spin coupled via a dipole-type interaction to two leads under a potential bias and (ii) the Anderson model, where a resonant level with an onsite repulsion is coupled to nonequilibrium leads. In the first case the dynamics of the tunneling system was investigated, recovering damped oscillations for weak-intermediate couplings with the bias playing a role analogous to that of the temperature in equilibrium systems. For the nonequilibrium Anderson model we focused our study on the resonant level population. Our method yields results in reasonable agreement with numerically exact Monte Carlo simulations for weak to intermediate onsite interactions U . For strong U deviations are observed. The results presented in Appendix D suggest that the deviations are related to memory and time-step truncation errors which we have been unable to control at the present time. Future work will be devoted to this issue.

Our path-integral formalism could be extended to handle bosonic degrees of freedom, representing, e.g., the nuclear coordinates of the molecular bridge in the Anderson model (Anderson-Holstein model). In particular, a phononic bath at thermal equilibrium could be easily incorporated, relying on the analytic form of the Feynman-Vernon influence functional.³⁰ Such a method, involving both fermionic and bosonic degrees of freedom, would become useful for exploring vibrational effects in electron conduction. Other models, e.g., the multilevel Anderson model or a multisite chain, could be treated by adopting the formulation of Appendix C. In summary, we expect this versatile numerically exact approach to become useful in complementing existing tools, increasing our understanding of nonequilibrium quantum transport and dissipation characteristics in many body models.

ACKNOWLEDGMENTS

D.S. acknowledges support from the Connaught grant. A.J.M. was supported by NSF under Grant No. DMR-0705847. D.R.R. would like to acknowledge the NSF for financial support. The authors acknowledge P. Werner for fruitful discussions and for providing the Monte Carlo data and M. Thorwart for useful correspondence and encouragement.

APPENDIX A: JUSTIFICATION OF THE TRUNCATION SCHEME

Here, we justify the breakup of the IF as prescribed by Eq. (8), demonstrating that the terms neglected account for interactions beyond the memory range τ_c . Consider for simplicity the functional

$$I(s_0^\pm, s_1^\pm, s_2^\pm, s_3^\pm, s_4^\pm) \approx I(s_0^\pm, s_1^\pm, s_2^\pm, s_3^\pm) \frac{I(s_1^\pm, s_2^\pm, s_3^\pm, s_4^\pm)}{I(s_1^\pm, s_2^\pm, s_3^\pm)}, \quad (\text{A1})$$

truncated here by following Eq. (8) with $N_s=3$. Using a cumulant expansion for the total IF,^{25,26} we write the IF as a product of n -body interaction terms, $I=I(2) \times I(3) \times I(4)$

$\times I(5)$, where each term is an exponent of a sum of the n -body terms. For example, $I(2) \sim e^{-\sum_{i,j} g_{i,j} s_{i,j}}$ with pairwise interactions $g_{i,j}$, $I(3) \sim e^{-\sum_{i,j,k} g_{i,j,k} s_{i,j,k}}$, incorporating ‘‘three-body’’ interactions $g_{i,j,k}$. Substituting this structure into Eq. (A1), we find that the following terms are not present on the right-hand side: The two- and three-body terms $g_{0,4}$, $g_{0,1,4}$, $g_{0,2,4}$, and $g_{0,3,4}$, four-body terms $g_{0,1,2,4}$, $g_{0,1,3,4}$, and $g_{0,2,3,4}$, and a five-body element $g_{0,1,2,3,4}$. These nonlocal interactions, connecting spins beyond the memory range specified, $N_s=3$, are assumed to be small and are therefore discarded in our truncation scheme. Larger memory blocks, connecting more distant time slices, may systematically be included until convergence with truncation of memory terms is reached.

To make this discussion concrete, consider a situation where nonequilibrium Coulomb gas behavior holds, as discussed in Refs. 32 and 33. In such cases, the total influence functional will be of the form $I \sim \exp[\sum_{i>j} C_0(|t_i-t_j|)]$, where $C_0(t) \propto \Delta\mu|t|$ up to logarithmic corrections. Consider now Eq. (8). Clearly the leading term contains all interactions between ‘‘charges’’ separated by a distance in time that does not exceed $|t_0-t_{N_s}|$, namely, $I(s_0^\pm, s_1^\pm, \dots, s_{N_s}^\pm) \sim \exp[\sum_{i>j}^{N_s} C_0(|t_i-t_j|)]$. Terms of the form $\frac{I(s_1^\pm, s_2^\pm, \dots, s_{N_s+1}^\pm)}{I(s_1^\pm, s_2^\pm, \dots, s_{N_s}^\pm)}$ include only interactions between charges interacting over the time intervals $|t_n-t_{N_s+1}|$, where $0 < n < N_s+1$, without double counting terms already contained in $I(s_0^\pm, s_2^\pm, \dots, s_{N_s}^\pm)$. This procedure is then iteratively continued until the complete influence functional is constructed. The error accrued originates from the neglect of terms in the exponent of the order $\Delta\mu\tau$, where $\tau=|t_a-t_b|$ and $b-a \geq N_s+1$. Thus, the procedure is rendered controlled and is expected to converge to the exact result as long as N_s is made large enough. It should be noted that the approach outlined here is more general than this and is expected to hold at short times or very large couplings where Coulomb gas behavior may break down, as discussed in Refs. 32 and 33.

APPENDIX B: EXTENSIONS OF THE IF TECHNIQUE TO FINITE TEMPERATURES

We present here the natural extension of our approach to finite temperature. The core of our numerical calculation is the IF, incorporating the Fermi sea degrees of freedom, e.g., Eq. (17) for the spin-fermion model or Eq. (25) for the Anderson model. Assuming for simplicity a single Fermi sea, consider the following IF-like object:

$$C_f = \text{Tr}_B[e^{M_1} e^{M_2} \rho_B], \quad (\text{B1})$$

where M_1 and M_2 are quadratic operators and $\rho_B = e^{-\beta H_B} / \text{Tr}_B[e^{-\beta H_B}]$, H_B is the bath Hamiltonian, Eq. (14). This correlation function can be expressed by single-particle operators,⁴⁹

$$C_f = \det[I - f(\epsilon) + e^{m_1} e^{m_2} f(\epsilon)]. \quad (\text{B2})$$

Here $f(\epsilon) = [1 + e^{\beta(\epsilon-\mu)}]^{-1}$ is the Fermi-Dirac distribution function, β is the inverse temperature, I is the unit operator, and m_1 and m_2 are single-particle operators corresponding to M_1 and M_2 , respectively. This expression can be trivially

extended to include more exponential terms, $e^{M_1}, e^{M_2}, \dots, e^{M_N}$, as necessary for the evaluation of the IF expression. For multiple-independent reservoirs, $\rho_B = \rho_L \otimes \rho_R$, the above relation can be generalized,

$$C_f = \text{Tr}_L \text{Tr}_R [e^{M_1} e^{M_2} \rho_L \otimes \rho_R] = \det\{ \{ [I_L - f_L(\epsilon)] \otimes I_R \} \times \{ [I_R - f_R(\epsilon)] \otimes I_L \} + e^{m_1} e^{m_2} [f_L(\epsilon) \otimes I_R] [f_R(\epsilon) \otimes I_L] \}. \quad (\text{B3})$$

Here I_α is the identity matrix for the α space; $\alpha=L,R$, and $f_\alpha(\epsilon) = [1 + e^{\beta\alpha(\epsilon - \mu_\alpha)}]^{-1}$. The above expressions reduce to the ones used in the text for $T=0$.

APPENDIX C: AN ALTERNATIVE FORMULATION: NONEQUILIBRIUM TRANSPORT THROUGH AN ANDERSON DOT

We present here an alternative formulation for calculating the dot properties in the SIAM without invoking the Hubbard-Stratonovich transformation. This formulation is based on a different Trotter decomposition than that used in Sec. IV. While the resulting expressions are more complex for the decomposition described here, it has the advantage that the resulting IF need not be updated each time step. Furthermore, since fewer terms of the Hamiltonian are split in the Trotter decomposition, it is possible that larger time steps may be taken with the decomposition presented here. Further work investigating this approach, which is not confined to the Anderson model, will be presented in a future work. We refer to the approach developed in Sec. IV as SIAM I, and to the method of this appendix as SIAM II.

We begin by partitioning Hamiltonian (18) as follows: H_0 includes the subsystem (dot) terms, and H_1 includes the two noninteracting leads (H_B) and system-bath couplings (H_{SB})

$$H^{AM} = H_0 + H_1, \quad H_1 = H_B + H_{SB},$$

$$H_0 = \sum_{\sigma} \epsilon_d n_{d,\sigma} + U n_{d,\uparrow} n_{d,\downarrow},$$

$$H_B = \sum_{\alpha,k,\sigma} \epsilon_k c_{\alpha,k,\sigma}^{\dagger} c_{\alpha,k,\sigma}, \quad H_{SB} = \sum_{\alpha,k,\sigma} V_{\alpha,k} c_{\alpha,k,\sigma}^{\dagger} d_{\sigma} + \text{H.c.} \quad (\text{C1})$$

Here $n_{d,\sigma} = d_{\sigma}^{\dagger} d_{\sigma}$ is the impurity number operator and $c_{\alpha,k,\sigma}^{\dagger}$ is a creation operator of an electron at the α lead with a spin σ and momentum k . Note that H_0 can be explicitly described by a four-state system, $|1\rangle = |0,0\rangle$, $|2\rangle = |\uparrow,0\rangle$, $|3\rangle = |\downarrow,0\rangle$, and $|4\rangle = |\uparrow,\downarrow\rangle$, corresponding to an empty dot, a single occupied dot of $\sigma = \uparrow, \downarrow$, and a double occupancy state. When U is very large ($U \rightarrow \infty$), we effectively have a three-state system since double occupancy becomes negligible. The energies of these four subsystem states are $E_1=0$, $E_{2,3}=\epsilon_d$, and $E_4=\epsilon_d + U$.

Consider the reduced density matrix $\rho_S = \text{Tr}_B\{\rho\}$ obtained by tracing the total density matrix ρ over the reservoir degrees of freedom. The time evolution of $\rho_S(t)$ is exactly given by

$$\rho_S(a, a', t) = \text{Tr}_B \langle a | e^{-iH^{AM}t} \rho(0) e^{iH^{AM}t} | a' \rangle, \quad (\text{C2})$$

where $|a\rangle$ and $|a'\rangle$ are subsystem states, as described above. Using the standard Trotter breakup, $e^{iHt} = (e^{iH\delta t})^N$, $\delta t = t/N$, and $e^{iH^{AM}\delta t} \approx e^{iH_0\delta t/2} e^{iH_1\delta t} e^{iH_0\delta t/2}$, we can rewrite Eq. (C2) in a path-integral formulation,

$$\begin{aligned} \rho_S(a, a', t) = & \int ds_0^+ \int ds_1^+ \cdots \int ds_{N-1}^+ \int ds_0^- \int ds_1^- \cdots \int ds_{N-1}^- \\ & \times \text{Tr}_B \{ \langle a | e^{-iH_0\delta t/2} e^{-iH_1\delta t} e^{-iH_0\delta t/2} | s_{N-1}^+ \rangle \\ & \times \langle s_{N-1}^+ | e^{-iH_0\delta t/2} e^{-iH_1\delta t} e^{-iH_0\delta t/2} | s_{N-2}^+ \rangle \cdots \\ & \times \langle s_0^+ | \rho(0) | s_0^- \rangle \cdots \langle s_{N-2}^- | e^{iH_0\delta t/2} e^{iH_1\delta t} e^{iH_0\delta t/2} | s_{N-1}^- \rangle \\ & \times \langle s_{N-1}^- | e^{iH_0\delta t/2} e^{iH_1\delta t} e^{iH_0\delta t/2} | a' \rangle \}, \quad (\text{C3}) \end{aligned}$$

where s_k are subsystem states. As an initial condition we may assume that $\rho(0) = \rho_B \rho_S(0)$ with the bath (B) uncoupled to the subsystem. We focus next on the following matrix elements in Eq. (C3):

$$\begin{aligned} G_{a,b}(\delta t) & \equiv \langle a | e^{-iH_0\delta t/2} e^{-iH_1\delta t} e^{-iH_0\delta t/2} | b \rangle \\ & = e^{-i(E_a + E_b)\delta t/2} \langle a | e^{-iH_1\delta t} | b \rangle. \quad (\text{C4}) \end{aligned}$$

To compute $\langle a | e^{-iH_1\delta t} | b \rangle$ note that it is advantageous to use again the Trotter splitting

$$\langle a | e^{-iH_1\delta t} | b \rangle \approx e^{-iH_B\delta t/2} \langle a | e^{-iH_{SB}\delta t} | b \rangle e^{-iH_B\delta t/2}. \quad (\text{C5})$$

We thus focus next on the matrix element

$$\hat{O}_{a,b} = \langle a | e^{-iH_{SB}\delta t} | b \rangle, \quad (\text{C6})$$

a quadratic operator in the space of the noninteracting electrons. It is useful to define the ‘‘composite’’ fermion $c_{0,\sigma} = \sum_{\alpha,k} V_{\alpha,k} c_{\alpha,k,\sigma}$, leading to $H_{SB} \equiv \sum_{\sigma} (c_{0,\sigma}^{\dagger} d_{\sigma} + d_{\sigma}^{\dagger} c_{0,\sigma})$. In this representation a direct expansion of the exponential gives

$$e^{\lambda H_{SB}} = I + (\cosh \lambda - 1) \hat{a}_2 + \sinh \lambda \hat{a}_1 \quad (\text{C7})$$

with $\lambda = -i\delta t$, $\hat{a}_1 = H_{SB}$, and $\hat{a}_2 = \sum_{\sigma} (d_{\sigma} d_{\sigma}^{\dagger} c_{0,\sigma}^{\dagger} c_{0,\sigma} + d_{\sigma}^{\dagger} d_{\sigma} + \text{H.c.})$. The operator [Eq. (C6)] is therefore of the form, $\hat{O}_{a,b} = \alpha + \beta c_{0,\sigma} + \beta' c_{0,\sigma}^{\dagger} + \gamma c_{0,\sigma} c_{0,\sigma} + \gamma' c_{0,\sigma}^{\dagger} c_{0,\sigma}^{\dagger}$, with constant coefficients α, β, γ . Substituting the pieces [Eqs. (C5)–(C7)] into Eq. (C4) yields

$$G_{a,b}(\delta t) \approx e^{-i(E_a + E_b)\delta t/2} e^{-iH_B\delta t/2} \hat{O}_{a,b} e^{-iH_B\delta t/2}, \quad (\text{C8})$$

incorporating linear combinations of bath operators $c_{0,\sigma}$ up to a quadratic order. Finally, we put all pieces together into Eq. (C3) and obtain the reduced dynamics

$$\begin{aligned} \rho_S(a, a', t) = & \int ds_0^+ \cdots \int ds_{N-1}^+ \int ds_0^- \cdots \int ds_{N-1}^- \langle s_0^+ | \rho_S(0) | s_0^- \rangle \\ & \times \exp[-i\delta t \sum_{j=1}^{N-1} E_{s_j^+} + i\delta t \sum_{j=1}^{N-1} E_{s_j^-} \\ & - i(E_a + E_{s_0^+})\delta t/2 + i(E_{a'} + E_{s_0^-})\delta t/2] \\ & \times \text{Tr}_B \{ (e^{-iH_B\delta t/2} \hat{O}_{a, s_{N-1}^+} e^{-iH_B\delta t} \hat{O}_{s_{N-1}^+, s_{N-2}^+} \\ & \times e^{-iH_B\delta t} \cdots \hat{O}_{s_1^+, s_0^+} e^{-iH_B\delta t/2}) \rho_B(0) (e^{-iH_B\delta t/2} \end{aligned}$$

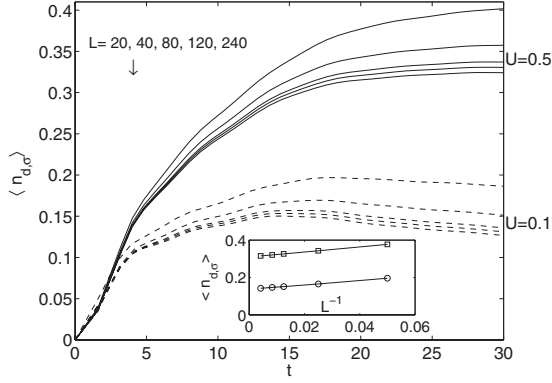


FIG. 6. Convergence of the dot occupancy with increasing number of bath states L . $E_d=0.3$, $\Gamma_\alpha=0.025$, $N_s=4$, and $\tau_c=3.2$. Full lines (top to bottom); $U=0.5$, $L=20, 40, 80, 120$, and 240 ; dashed lines (top to bottom): $U=0.1$, $L=20, 40, 80, 120$, and 240 . Inset: data as a function of L^{-1} at $t=20$, $U=0.5$ (square) and $U=0.1$ (circle).

$$\times \hat{O}_{s_0 \rightarrow 1}^- e^{-iH_B \delta t} \hat{O}_{s_1 \rightarrow 2}^- e^{-iH_B \delta t} \dots \hat{O}_{s_{N-1} \rightarrow a}^- e^{-iH_B \delta t/2} \}. \quad (\text{C9})$$

Identifying the integrand as the IF, we can use the approach of Sec. II, define the truncated IF I_s , and iteratively propagate the reduced density matrix to long times.

The approach developed here (SIAM II) has three main advantages over the method described in the main text (SIAM I), see Sec. IV. First, since the present method does not rely on the Hubbard-Stratonovich transformation it can be applied to general many body interaction Hamiltonians while SIAM I is restricted to the Anderson model. Second, since the Trotter error in SIAM II is due to system-bath factorization, rather than one-body-many-body splitting as in SIAM I, the method described here should be beneficial in calculating dynamics of weakly coupled system-bath models with arbitrarily large many body (local) interactions. Finally, this method also suggests a computational advantage over

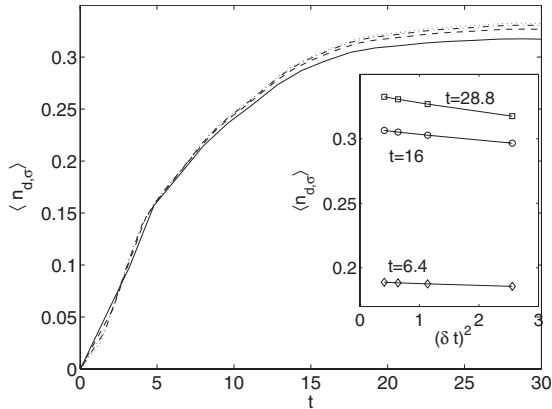


FIG. 7. Convergence of dot occupancy reducing the time step $\delta t = \tau_c / N_s$. $E_d=0.3$, $U=0.5$, $\Gamma_\alpha=0.025$, $\tau_c=3.2$, $L=120$, and $\delta t=1.6$ (full); $\delta t=1.07$ (dashed); $\delta t=0.8$ (dashed-dotted); and $\delta t=0.64$ (dotted). Inset: data as a function of $(\delta t)^2$ for three representative times.

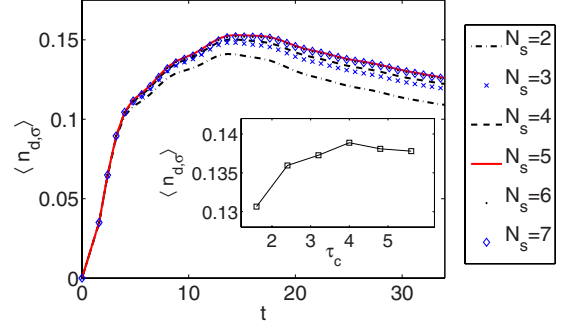


FIG. 8. (Color online) Convergence of dot occupancy with increasing memory size τ_c . $E_d=0.3$, $U=0.1$, $\Gamma_\alpha=0.025$, $L=120$, and $\delta t=0.8$. $N_s=2$ (dashed-dotted); $N_s=3$ (x); $N_s=4$ (dashed); $N_s=5$ (full); $N_s=6$ (dotted); and $N_s=7$ (\diamond) Inset: dot population vs τ_c at a specific time, $t=12$.

SIAM I since the IF here [integrand of Eq. (C9)] is *time independent*, unlike the IF of Eq. (25) which needs to be recalculated at each time step.

APPENDIX D: CONVERGENCE ANALYSIS FOR THE ANDERSON MODEL

There are three separate sources of systematic error within our approach. (i) *Bath discretization error*. The electronic reservoirs are explicitly included in our simulations, and we use bands extending from $-D$ to D with a finite number of states per bath per spin (L). This is in contrast to standard approaches where a wideband limit is assumed and analytical expressions for the reservoirs Green's functions are adopted.^{12,27,44} (ii) *Trotter error*. The time discretization error originates from the approximate factorization of the total Hamiltonian into the noncommuting H_0 (two-body) and H_1 (many-body) terms, see text after Eq. (20). While for $U \rightarrow 0$ and for small time steps $\delta t \rightarrow 0$ the decomposition is exactly satisfied, for large U one should go to a sufficiently small time step in order to avoid significant error buildup. (iii) *Memory error*. Our approach assumes that bath correlations exponentially decay resulting from the nonequilibrium condition $\Delta\mu \neq 0$. Based on this crucial element, the influence functional may be truncated to include only a finite number of fictitious spins N_s , where $\tau_c = N_s \delta t \sim 1/\Delta\mu$. The total IF is retrieved by taking the limit $N_s \rightarrow N$, ($N = t/\delta t$).

These three errors can be systematically eliminated by increasing the number of bath states, choosing a small enough time step, and adopting a sufficiently long memory time. Note however that the last two strategies are linked: increasing τ_c essentially means increasing the time step since the memory length is restricted to small values $N_s=4-6$ for practical-computational reasons. Thus, as in standard QUAPI,²⁴ one should find an optimal balance between the time-step error and the memory size that correctly represents the dynamics. Reference 50 suggests a systematic approach for reaching convergence using the QUAPI method, eliminating the Trotter discretization error and the memory truncation inaccuracy by extrapolating the data to vanishing time step and to infinite memory time.

A similar idea can be adopted here. First the bath finite-size error can be eliminated by systematically increasing the number of fermions at each lead. As an example, Fig. 6 presents the dot population for $U=0.1$ and $U=0.5$ taking $L=20, 40, 80, 120,$ and 240 (top to bottom). The inset shows that convergence can be reached, and that the occupancy is systematically decreasing with L . Next, the Trotter error can be eliminated by extrapolating the data to the $\delta t \rightarrow 0$ limit. Figure 7 presents as an example the occupancy for $\Delta\mu=0.4$ using $\tau_c=3.2$, and $\delta t=1.6, 1.05, 0.8, 0.64$. The inset manifests convergence as a function of $(\delta t)^2$. Note that in the asymptotic limit the data points are slightly enhanced, prac-

tically canceling the effect of the bath discretization. Finally, the memory effect is analyzed in Fig. 8. For the parameters employed here ($E_d=0.3, U=0.1, \Gamma_\alpha=0.025, \Delta\mu=0.4$) convergence is arrived at $\tau_c \sim 4$ (inset), in agreement with the rough estimate $\tau_c \sim 1/\Delta\mu$. We have not been able to obtain full convergence for $U/\Gamma \geq 3$.

Using this analysis, we have recalculated Fig. 4 extrapolating our data to (i) $L \rightarrow \infty$, (ii) $\delta t \rightarrow 0$, and (iii) $\tau_c \rightarrow \infty$. Since the extrapolations (i) and (ii), bring about counter contributions, see Figs. 6 and 7, the overall effect of the bath-time step-memory extrapolations on the occupation is rather small, and Fig. 4 remains essentially intact.

-
- ¹A. J. Leggett, S. Chakravarty, A. T. Dorsey, M. P. A. Fisher, A. Garg, and W. Zwerger, *Rev. Mod. Phys.* **59**, 1 (1987).
- ²U. Weiss, *Quantum Dissipative Systems* (World Scientific, Singapore, 1993).
- ³I. Bloch, J. Dalibard, and W. Zwerger, *Rev. Mod. Phys.* **80**, 885 (2008).
- ⁴I. L. Aleiner, P. W. Brouwer, and L. I. Glazman, *Phys. Rep.* **358**, 309 (2002).
- ⁵*Molecular Nanoelectronics*, edited by M. A. Reed and T. Lee (American Scientific, Stevenson Ranch, CA, 2003).
- ⁶L. P. Kadanoff and G. Baym, *Quantum Statistical Mechanics* (Benjamin, New York, 1962); L. V. Keldysh, *Zh. Eksp. Teor. Fiz.* **47**, 1515 (1964).
- ⁷A.-P. Jauho, N. S. Wingreen, and Y. Meir, *Phys. Rev. B* **50**, 5528 (1994).
- ⁸N. S. Wingreen and Y. Meir, *Phys. Rev. B* **49**, 11040 (1994).
- ⁹K.-c. Chou, Z.-b. Su, B.-l. Hao, and L. Yu, *Phys. Rep.* **118**, 1 (1985).
- ¹⁰H. Haug and A. P. Jauho, *Quantum Kinetics in Transport and Optics of Semiconductors* (Springer, Germany, 1996).
- ¹¹R. Egger, L. Mühlbacher, and C. H. Mak, *Phys. Rev. E* **61**, 5961 (2000).
- ¹²L. Mühlbacher and E. Rabani, *Phys. Rev. Lett.* **100**, 176403 (2008).
- ¹³M. Schiró and M. Fabrizio, *Phys. Rev. B* **79**, 153302 (2009).
- ¹⁴M. Gell-Mann and M. L. Goldberger, *Phys. Rev.* **91**, 398 (1953).
- ¹⁵T. N. Todorov, G. A. D. Briggs, and A. P. Sutton, *J. Phys.: Condens. Matter* **5**, 2389 (1993).
- ¹⁶S. Hershfield, *Phys. Rev. Lett.* **70**, 2134 (1993); A. Schiller and S. Hershfield, *Phys. Rev. B* **51**, 12896 (1995).
- ¹⁷P. Mehta and N. Andrei, *Phys. Rev. Lett.* **96**, 216802 (2006); B. Doyon and N. Andrei, *Phys. Rev. B* **73**, 245326 (2006).
- ¹⁸J. E. Han, *Phys. Rev. B* **73**, 125319 (2006); **75**, 125122 (2007); J. E. Han and R. J. Heary, *Phys. Rev. Lett.* **99**, 236808 (2007).
- ¹⁹A. Dhar, D. Sen, and D. Roy, *Phys. Rev. Lett.* **101**, 066805 (2008); D. Roy, A. Soori, D. Sen, and A. Dhar, *Phys. Rev. B* **80**, 075302 (2009).
- ²⁰A. Nishino, T. Imamura, and N. Hatano, *Phys. Rev. Lett.* **102**, 146803 (2009).
- ²¹F. B. Anders and A. Schiller, *Phys. Rev. Lett.* **95**, 196801 (2005); *Phys. Rev. B* **74**, 245113 (2006); F. B. Anders, *Phys. Rev. Lett.* **101**, 066804 (2008).
- ²²S. R. White and A. E. Feiguin, *Phys. Rev. Lett.* **93**, 076401 (2004).
- ²³F. Heidrich-Meisner, A. E. Feiguin, and E. Dagotto, *Phys. Rev. B* **79**, 235336 (2009).
- ²⁴D. E. Makarov and N. Makri, *Chem. Phys. Lett.* **221**, 482 (1994); N. Makri and D. E. Makarov, *J. Chem. Phys.* **102**, 4600 (1995); **102**, 4611 (1995); N. Makri, *J. Math. Phys.* **36**, 2430 (1995).
- ²⁵N. Makri, *J. Phys. Chem. B* **103**, 2823 (1999).
- ²⁶N. Makri, *J. Chem. Phys.* **111**, 6164 (1999).
- ²⁷S. Weiss, J. Eckel, M. Thorwart, and R. Egger, *Phys. Rev. B* **77**, 195316 (2008); J. Eckel, F. Heidrich-Meisner, S. G. Jakobs, M. Thorwart, M. Pletyukhov, and R. Egger, *New J. Phys.* **12**, 043042 (2010).
- ²⁸R. Blankenbecler, D. J. Scalapino, and R. L. Sugar, *Phys. Rev. D* **24**, 2278 (1981).
- ²⁹Simulations were performed here using the MATLAB compiler and the Parallel Computing Toolbox of MATLAB.
- ³⁰R. P. Feynman and A. R. Hibbs, *Quantum Mechanics and Path Integrals* (McGraw-Hill, New York, 1965).
- ³¹A. Mitra and A. J. Millis, *Phys. Rev. B* **72**, 121102(R) (2005).
- ³²D. Segal, D. R. Reichman, and A. J. Millis, *Phys. Rev. B* **76**, 195316 (2007).
- ³³A. Mitra and A. J. Millis, *Phys. Rev. B* **76**, 085342 (2007).
- ³⁴R. M. Lutchyn, L. Cywinski, C. P. Nave, and S. Das Sarma, *Phys. Rev. B* **78**, 024508 (2008).
- ³⁵J. Paaske, A. Rosch, and P. Wolfle, *Phys. Rev. B* **69**, 155330 (2004); J. Paaske, A. Rosch, J. Kroha, and P. Wolfle, *ibid.* **70**, 155301 (2004).
- ³⁶A. C. Hewson, *The Kondo Problem to Heavy Fermions* (Cambridge University Press, Cambridge, England, 1993).
- ³⁷T. K. Ng, *Phys. Rev. B* **51**, 2009 (1995); **54**, 5814 (1996).
- ³⁸H. J. Lee and R. Bulla, *Eur. Phys. J. B* **56**, 199 (2007).
- ³⁹I. Klich, in *Quantum Noise in Mesoscopic Systems*, edited by Yu. V. Nazarov (Kluwer, Dordrecht, 2003).
- ⁴⁰K. Byczuk and D. Vollhardt, *Phys. Rev. B* **77**, 235106 (2008).
- ⁴¹P. Anders, E. Gull, L. Pollet, M. Troyer, and P. Werner, *Phys. Rev. Lett.* **105**, 096402 (2010).
- ⁴²P. W. Anderson, *Phys. Rev.* **124**, 41 (1961).
- ⁴³J. E. Hirsch, *Phys. Rev. B* **28**, 4059 (1983).
- ⁴⁴P. Werner, A. Comanac, L. de Medici, M. Troyer, and A. J. Millis, *Phys. Rev. Lett.* **97**, 076405 (2006); E. Gull, P. Werner, A. Millis, and M. Troyer, *Phys. Rev. B* **76**, 235123 (2007); P. Werner, T. Oka, and A. J. Millis, *ibid.* **79**, 035320 (2009).

- ⁴⁵P. Werner, T. Oka, M. Eckstein, and A. J. Millis, *Phys. Rev. B* **81**, 035108 (2010).
- ⁴⁶L. Muehlbacher, D. Urban, and A. Komnik, [arXiv:1007.1793](https://arxiv.org/abs/1007.1793) (unpublished).
- ⁴⁷P. Reddy, S. Y. Jang, R. A. Segalman, and A. Majumdar, *Science* **315**, 1568 (2007).
- ⁴⁸H. Wang and M. Thoss, *J. Chem. Phys.* **119**, 1289 (2003); **131**, 024114 (2009).
- ⁴⁹D. A. Abanin and L. S. Levitov, *Phys. Rev. Lett.* **94**, 186803 (2005).
- ⁵⁰J. Eckel, S. Weiss, and M. Thorwart, *Eur. Phys. J. B* **53**, 91 (2006).